Title Page

LRP6 modulates the phosphorylation of Cx43 via $G\alpha_s$ in ventricular tachycardia of myocardial infarction

Xu-min Zhang MD[1], Ya-ling Liu MD[2], Ying Cai MD[1], Ying Hao MD[1], Sheng Kang MD PhD[1]

1. Department of Cardiology, Shanghai East Hospital, School of Medicine, Tongji University, Jimo Road 150, Shanghai 200120, China
2. Department of Anesthesiology, Renji hospital, School of Medicine, Shanghai Jiaotong University, Pujian Road 160, Shanghai, 200127, China

Xu-min Zhang and Ya-ling Liu are joint first authors.

Corresponding Author Sheng Kang MD PhD

Department of Cardiology

Shanghai East Hospital

School of Medicine, Tongji University

Jimo Road 150, Shanghai 200120, China

e-mail: kangsheng2008@163.com

Running title LRP6, Cx43 and VT

Tables 2

Figures 7

Total words 5686

Abstract

Background Ventricular tachycardia (VT) and ventricular fibrillation are the most causes of early death in patients with myocardial infarction (MI). This study was aimed to explore whether LRP6 and its upstream genes circRNA1615 and miR-152-3p modulated the phosphorylation of Connexin-43 (Cx43) via $G\alpha_s$ in VT of MI.

Method we constructed the hypoxia cardiomyocyte model and AMI mice, and explored the modulation relationship of LRP6 and its upstream genes circRNA1615 and miR-152-3p. In addition, the immunoblot analysis with monoclonal and polyclonal antibodies were used to detect whether LRP6 and Cx43 were phosphorylated, further investigated that the LRP6 regulated the phosphorylation of its downstream target Cx43 via G-protein alpha subunit $G\alpha_s$ by using cell transfection, FISH assay, HE staining, RT-qPCR, and Western blot techniques.

Result LRP6 mRNA expression was significantly reduced in AMI group compared with the control group. Hypoxia could inhibit the protein and phosphorylation levels of LRP6 and Cx43. The expression of circRNA1615 in AMI mice was significantly decreased, but overexpression of circRNA1615 significantly reversed the inhibitory effect of AMI. Also overexpression of circRNA1615 could weaken the effect of miR-152-3p mimic, and the miR-152-3p mimic increased the hypoxia injury of LRP6 and Cx43, further LRP6 interference fragments could aggravate hypoxia injury of Cx43. The overexpression of LRP6 could significantly increase the protein level and phosphorylation level of Cx43, but the interference with LRP6 showed the opposite trend. Noticeably, the interference with $G\alpha_s$ weakened the protein and phosphorylation levels of Cx43, however, the interference with LRP6 and $G\alpha_s$ further inhibited the protein and phosphorylation levels of Cx43. Finally, the transcriptions of circRNA1615 and LRP6 were inhibited in AMI, but the transcription of miR-152-3p was promoted, and the overexpression of circRNA1615 could weaken the damage effect and VT of AMI.

Conclusion LRP6 and its upstream genes circRNA1615 and miR-152-3p modulated the phosphorylation of Cx43 via $G\alpha_s$ in VT of MI.

Keywords: LRP6, $G\alpha_s$, Cx43, phosphorylation, ventricular tachycardia

Introduction

More than 50% patients died of fatal ventricular arrhythmias in acute myocardial infarction (AMI), particularly in ventricular tachycardia(VT) and ventricular fibrillation, are the most causes of early death.[1] The previous studies found that (1) after myocardial infarction (MI), the density of cardiac sympathetic nerve in the peri-infarcted zone was increased and activated, and the automaticity of cardiomyocytes in the peri-infarcted zone was significantly higher than that in other areas,[2] which was likely to become an ectopic excitatory focal point to release impulses, causing arrhythmias; (2) the electrical remodeling of cardiomyocytes was also observed in both infarcted and non-infarcted areas, showing the changes of cardiac electrophysiological parameters.[3] The electrical remodeling of cardiomyocytes would be the important mechanism of ventricular arrhythmias in AMI. (3) Cardiac anatomical tissue remodeling was an critical matrix for the occurrence and maintenance of ventricular arrhythmias in chronic MI. Myocardial fibrosis, collagen deposition, cardiomyocyte hypertrophy, scar tissue formation, and gap junction remodeling (characterized by the spatial distribution and quantitative abnormality of gap junction protein Connexin (Cx), especially Cx43 in the infarcted area affected the formation and conduction of cardiac electrical activity, and then promoted the occurrence of arrhythmia.[4-6]

In the traditional theory, sympathetic innervation regulated the expression of myocardial ion channels, anatomical tissue remodeling, especially Cx43 remodeling also directly influenced myocardial electrical remodeling, and the distribution of sympathetic nerve might also be closely related to the expression of Cx43. However, the mechanisms of interaction between the three factors were not clear, and the elucidation of these mechanisms will provide a new target for drug treatment of ventricular arrhythmias after MI.

Noticeably, low-density lipoprotein receptor-related protein 6 (LRP6) is a member of the low-density lipoprotein receptors (LDLRs) family and accumulating evidence points to the critical role of LRP6 in cardiovascular health and homeostasis.[7,8] Importantly, the hearts of conditional cardiac-specific Lrp6-knockout mice consistently exhibit overt reduction of Cx43 gap junction plaques without any abnormality in Wnt signaling and are predisposed to lethal ventricular arrhythmias.[9] Interestingly, LRP6 mediates cAMP generation by G protein-coupled receptors through regulating the membrane targeting of Ga_s.[10] Further in our previous researches, screening and identification of the upstream gene circRNA1615 would target LRP6. Also circRNA1615 could regulate the expression of LRP6 mRNA through sponge adsorption of miR-152-3p, and finally controlled the pathological process of MI.[12]

Therefore, this study was aimed to explore whether LRP6 and its upstream genes circRNA1615 and miR-152-3p modulate the phosphorylation of Cx43 via Gα_s in VT of MI.

Materials and methods

Ethics statement

Experimental procedures in this study were performed with approval of the ethics board of the Laboratory Animal Research Center, Tongji University (No. TJTJ00621401). All animal experiments were conducted in strict accordance with the recommendations in the Guide for the Care and Use of Laboratory Animals of the National Institutes of Health. Adequate measures were taken to minimize the suffering of animals in this study.

Construction of AMI mouse model

Twenty-four specific pathogen free (SPF) male C57BL/6J mice were acquired from Beijing Vital River Laboratory Animal Technology Co., Ltd. (Beijing, China), among which eight mice were grouped as the normal control, and the remaining sixteen mice were reserved for the establishment of AMI models. All mice were housed in an SPF animal laboratory on a normal diet with relative humidity of 60% - 65% and temperature at 22° C - 25° C.

Then the lentiviral vector (1×10^9 pfu/mouse, Shanghai GenePharma Co., Ltd., Shanghai, China) harboring pLVX-Puro-circRNA1615 was transfected into the C57BL/6 mice of the experimental group *via* the intramyocardial injection. These mice were fasted overnight before AMI induction. Mice were anesthetized using an intraperitoneal injection with pentobarbital sodium (0.05 mg/g, P3761, Sigma-Aldrich, St. Louis, MO, USA). Next, the thoracic cavity was exposed and the left coronary artery descending branch (2 mm at the lower border of the left atrium junction) was ligated using a 7-0 surgical suture to establish a mouse model of MI. The eight mice from the control group underwent the aforementioned surgical procedures without ligation. After surgery, the thoracic cavity was sutured and the condition and wound infection of the mice were observed. At 2 days after surgery, the mice were performed by cervical dislocation method for euthanasia. Finally, the hearts were collected and fixed with paraformaldehyde for subsequent studies.

Culture of cardiomyocytes and establishment of a hypoxic cell model

The mouse cardiomyocytes (Pricells, Wuhan, China; MIC-CELL-0006) were cultured using the Dulbecco's modified Eagle's medium (DMEM, Gibco™, Thermo Fisher, Waltham, MA, USA) containing a combination of 10% fetal bovine serum (FBS, Excell Bio, Genetimes, Shanghai, China), 100 U/mL penicillin and 100 μg/mL streptomycin in an incubator at 37° C with 5% CO_2 and under saturated humidity. The cells were seeded in a 6-well plate and cultured for 24 hours, they were exposed to hypoxia to induce AMI by culture under anoxic conditions with 93% N_2, 2% O_2, and 5% CO_2. Those cells cultured under normal conditions were subsequently used as control. After 24 hours of culture, the subsequent experimentation was conducted.

Cell transfection

The control pLVX-Puro lentivirus and circRNA1615 overexpression lentivirus were constructed by Obio Technology Company (Shanghai, China). The Liposome 3000 reagent was used to transfect the miR-152-3p mimic (5'-UCAGUGCAUGACAGAACUUGG-3'), inhibitor (5'-CCAAGUUCUGUCAUGCACUGA-3') and its negative control. Cells were transfected with control pcDNA3.1 plasmid and LRP6 overexpression plasmid (Generay Technologies, Shanghai, China) using Liposome 3000 reagent. Small interfering RNAs (Shanghai GenePharma Co., Ltd, China) were transfected into the mouse cardiomyocytes using Lipofection 3000 reagent. Empty vector and nonspecific siRNA (siNC) were used as negative controls. All the sequences of siRNAs were listed in Table 1.

FISH assay

FISH assay was conducted to determine the subcellular localization of circRNA1615. Briefly, the slide was placed in a 6-well plate, in which the cardiomyocytes were inoculated. After 1 day of incubation to attain 80% cell confluence, the cells were rinsed with PBS and fixed using 1 mL of 4% paraformaldehyde. After treatment with glycine and the acetylation reagent, the cells were probed with 250 μL of the pre-hybridization solution for 1 hour at 42° C. After elimination of the pre-hybridization solution, 250 μL of the hybridization solution (300 ng/mL) containing the circRNA1615 specific probe was added for overnight hybridization at 42° C. After three rinses using PBS and Tween-20 (PBST), the cells were stained using 4',6-diamidine-2-phenylindole (DAPI) diluted by PBST (1 : 800) in the 24-well plate for 5 min. After sealing with an anti-fluorescence quenching agent, the cells were observed and photographed under a fluorescence microscope (Olympus, Japan) in five randomly selected fields.

HE staining

The myocardial tissues of the mice were fixed in 4% paraformaldehyde (P0099, Beyotime, Shanghai, China) for 24 hours, and then conventionally dehydrated with gradient alcohol of variable concentrations (70%, 80%, 90%, 95%, 100% respectively) for 5 min/time. The sections were cleared using xylene 2 times, embedded in paraffin, and sectioned systematically for a thickness of 4 µm. After baking at 60° C for 1 hour, the sections were dewaxed using xylene, dehydrated by gradient ethanol, stained with hematoxylin for 10 min, and finally differentiated using 1% hydrochloric acid alcohol for 20 seconds. Then, 1% ammonia water was supplemented to develop a blue color gamut for 30 seconds. Eosin staining was performed on the sections for 3 min, which were then dehydrated using gradient ethanol, cleared with xylene and mounted with neutral gum. Finally, the section was observed under optical microscope (Olympus, Tokyo, Japan).

RT-qPCR

The cardiomyocytes were collected, and the total RNA content was extracted with TRIzol (Invitrogen™, Carlsbad, CA, USA). First strand cDNA was synthesized using the first strand cDNA synthetase according to the provided instructions of the First Strand cDNA Synthesis Kit (Takara, Tokyo, Japan). The gene expression was assessed by real-time qPCR using the SYBR Premix Ex Taq kit (Takara, Tokyo, Japan). Real time qPCR was conducted on an ABI Prism 7500 Fast Real-Time PCR system (Applied Biosystems, MA, USA). The gene expression was calculated based on the $2^{-\Delta\Delta Ct}$ methods with U6 and glyceraldehyde-3-phosphate dehydrogenase (GAPDH) serving as the endogenous control. As for RNA expression pattern in the mouse myocardial tissue samples, 0.1 g tissue samples were collected, and grounded at 4°C using a tissue grinder (KZ-II, Servicebio, Wuhan, Hubei, China), and the RNA content was extracted using TRIzol (Invitrogen™, Carlsbad, CA, USA) in compliance with the aforementioned procedure. All the primer sequences were listed in Table 2.

Western blot assay

The total protein content was extracted using the radioimmunoprecipitation assay lysis buffer (R0010, Solarbio, Beijing, China). Cell lysis was collected in an eppendorf tube, and then lysed over ice for 30 min. After centrifugation at 13,000 × g for 10 min at 4° C, the supernatant was collected, and placed over ice, and the protein concentration was determined using a bicinchoninic acid protein concentration assay kit (P0011, Beyotime, Shanghai, China). Polyacrylamide gel electrophoresis was conducted for protein separation, and the protein was transferred to a 0.2 μm polyvinylidene fluoride membrane (ISEQ10100, Merck Millipore, Billerica, MA, USA) by the wet transfer. Membrane blockade was conducted with the Tris-Buffered Saline Tween-20 (TBST) (D8340, Solarbio Life Sciences Co., Ltd., Beijing, China) containing 5% skim milk powder for 1 hour at ambient temperature. The primary antibodies diluted by the addition of TBST containing 1% skim milk powder were added in a drop-wise manner and incubated with the membrane at 4°C overnight, including anti-LRP6 (Invitrogen; AB_2691702), phospho-LRP6 (Ser1490) rabbit polyclonal antibody (Invitrogen; AB_2815875), anti-Cx43 (Sigma-Aldrich; AB1728), anti-Gαs (Sigma-Aldrich; 06-237), and anti-GAPDH antibody (Cell Signaling Technology; #5174). Although it reported a mouse monoclonal antibody (clone CX-1B1) generated against amino acids 360 to 376 (Zymed Laboratories Inc, South San Francisco, Calif) to identify selectively nonphosphorylated Cx43 binding,[12-14] we decided to use a phospho-connexin 43 (Ser368) rabbit polyclonal antibody (Invitrogen; AB_2533845). On the following day, the secondary antibody horseradish peroxidase-labeled antibody to immunoglobulin G (IgG) (Beyotime, Shanghai, China; A0216, A0208) diluted by the supplementing TBST containing 1% skim milk powder was added and incubated with the experimental membrane for 1 hour at ambient temperature, followed by development using a digital chemiluminometer (C-DiGit® Blot Scanner, Li-Cor, NE, USA) and analysis using the Image J software. GAPDH served as the internal reference, and the ratio of the gray value of the target band to that of the internal reference band was regarded as the relative expression of the protein.

Statistical analysis

GraphPad Prism 8.0.2 (GraphPad Software, San Diego, CA, USA) was used for statistical analysis. The normal distribution and homogeneity of variance were tested accordingly. For data conforming to normal distribution and homogeneity of variance, the continuous variables were summarized as mean ± standard deviation. Comparisons between two groups were analyzed by unpaired *t* test, while comparisons among multiple groups were performed using one-way analysis of variance (ANOVA) with the Tukey's post hoc test. A value of $p < 0.05$ was considered to be statistically significant.

Results

The injury of myocardial tissue caused by hypoxia was identified with HE staining in Fig.1(A), and it was observed that the cell arrangements of the normal control were clear and uniform, the transverse cells were neatly arranged, and the intercellular space was uniform; the muscle fibers were intact and consistent, showing the morphology of normal cardiomyocytes. On the other hand, in the hypoxia group, the arrangement of cells was disordered, the myocardial fibers became thicker, the gap became larger and confused, which showed the abnormal morphology of cardiomyocytes. In Fig.1(B), LRP6 mRNA expression was significantly reduced in AMI compared with the normal control. Similarly, hypoxia could inhibit the phosphorylation levels of LRP6 and Cx43 in Fig.1(C). Notably, VT was frequently occurred in AMI model compared with normal control in Fig.1(D).

In fluorescence staining of circRNA1516 of Fig2(A), the hypoxia model of primary mouse cardiomyocytes was established, and the localization of circRNA1615 was determined by fluorescence in situ hybridization (FISH). The result showed that hypoxia inhibited its expression. Further the AMI model was established in C57 mice. Similarly, it showed that the expression of circRNA1615 in AMI mice was significantly decreased in Fig2(B), while overexpression of circRNA1615 was transfected into AMI mice, it showed that circRNA1615 expression was significantly reduced in the tissues of AMI mice, but overexpression of circRNA1615 significantly reversed the inhibitory effect of AMI on circRNA1615 expression in Fig2(C).

In Fig.3(A, B), after the cells were treated with inhibitor and mimics of miR-152-3p, the expression efficiency of miR-152-3p was detected by PCR assay, and it showed that the effects of interference and overexpression of miR-152-3p were visible. In Fig.3(C, D), the phosphorylation levels of LRP6 and Cx43 decreased in hypoxic condition. The inhibitor of miR-152-3p could block the hypoxia injury, but the miR-152-3p mimic further increased the hypoxia injury. Overexpression of circRNA1615 could weaken the effect of miR-152-3p mimic, while the interference of circRNA1615 would reduce the effect of miR-152-3p inhibitor.

The efficiency verification of interference with LRP6 were displayed in Fig.4(A and B), and the verification of overexpression efficiency of LRP6 was showed in Fig.4(C and D). In Fig.4 (E), the hypoxia condition inhibited the expression and phosphorylation of LRP6 and Cx43. LRP6 interference fragments could further aggravate hypoxia injury. The addition of LRP6 overexpression plasmid significantly reversed the effect of hypoxia. Compared with the interference of LRP6 alone, the addition of circRNA1615 overexpression to the cells of LRP6 interference fragments tended to increase but not significantly. While the addition of circRNA1615 interference fragments in the case of LRP6 overexpression could significantly diminish the protective effect of LRP6.

Noticeably, the overexpression of LRP6 significantly elevated the protein level and phosphorylation level of Cx43, but the interference with LRP6 showed the opposite trend in Fig.5(A). Importantly, the interference with Gα_s weakened the protein and phosphorylation levels of Cx43, however, the interference with LRP6 and Gα_s further inhibited the protein level and phosphorylation level of Cx43 in Fig.5(B).

As mentioned above, in the HE staining and fluorescence staining of Fig.6(A), it showed that the staining of circRNA1615 decreased in AMI, but rose significantly after the overexpression of circRNA1615, and the tissue damage was improved, and the overexpression of circRNA1615 could weaken the damage effect of AMI. In Fig.6(B), VT was frequently occurred in AMI model, conversely, it was rarely in the overexpressed circRNA1615 group and normal control group. In Fig.6(C and E), the transcriptions of circRNA1615 and LRP6 were inhibited in AMI model, but the transcription of miR-152-3p was promoted in Fig.6(D). In addition, the protein and phosphorylation levels of LRP6 and Cx4 were reduced in AMI model, and the overexpression of circRNA1615 could considerably decrease the disruption of AMI in Fig.6(F).

Discussion

The principal results of present study showed that hypoxia could inhibit the phosphorylation levels of LRP6 and Cx43. The overexpression of LRP6 could significantly increase the protein level and phosphorylation level of Cx43. Noticeably, the interfering with Gα_s weakened the protein and phosphorylation level of Cx43, however, the interference with LRP6 and Gα_s further inhibited the protein level and phosphorylation level of Cx43. Finally, the transcriptions of circRNA1615 and LRP6 were inhibited in AMI, but the transcription of miR-152-3p was promoted, and the overexpression of circRNA1615 could weaken the damage effect and ventricular tachycardia of AMI.

Gap junctions are necessary to coordinate cell function by passing electrical current flow between heart and nerve cells or by allowing exchange of chemical signals and energy substrates. Connexin expression is affected by age and gender as well as several pathophysiological alterations such as hypertension, hypertrophy, diabetes, hypercholesterolemia, ischemia, post-MI remodeling or heart failure, and post-translationally connexins are modified by phosphorylation/de-phosphorylation and nitros(yl)ation which can modulate channel activity.[15] Cx43 dephosphorylation in synchronously contracting myocytes during ischemia is reversible, independent of hypoxia, and closely associated with cellular ATP levels. Cx43 became profoundly dephosphorylated during hypoxia only when glucose supplies were limited and was completely rephosphorylated within 30 minutes of reoxygenation. recovery of phosphoCx43 accompanied restoration of ATP.[16] The different phases of uncoupling during ischemia can be clearly discerned. With this approach, uncoupling and Cx43 dephosphorylation were first detected at about the same time after the onset of ischemia and progressed with a similar time course. Reperfusion after an interval of ischemia sufficient to cause both uncoupling and Cx43 dephosphorylation led to at least partial restoration of the control level of phosphorylated Cx43 in hearts that recovered contractile activity, whereas further dephosphorylation of Cx43 occurred in hearts that failed to recover. With uncoupling, however, there was progressive loss of Cx43 signal at sites of intercellular apposition concomitant with a marked increase in nonphosphorylated Cx43.[13] During ischemia, dephosphorylated Cx43 fluorescence increased markedly in the ischemic zone relative to the nonischemic zone, and this difference persisted during early reperfusion. Cx43 dephosphorylation perpetuates slow conduction and increases susceptibility to reentrant arrhythmias during early reperfusion.[14] In our findings, hypoxia could inhibit the phosphorylation levels of LRP6 and Cx43. LRP6 mRNA expression was significantly reduced in AMI model compared with the healthy control. The expression of circRNA1615 in AMI mice was significantly decreased, but overexpression of circRNA1615 significantly reversed it. Notably, VT was frequently occurred in AMI model vs. normal control (Fig.1).

In our early research,[11] it was constructed the modulation network of circRNA-miRNA-LRP6 by bioinformatics analysis; then screening and identification of the upstream gene circRNA1615 would target LRP6, and circRNA1615 could regulate the expression of LRP6 through sponge adsorption of miR-152-3p in the RIP experiments and the double luciferase reporter gene assay. In this study, we further validated that compared with the control group, LRP6 mRNA and circRNA1615 expression were significantly reduced in AMI group. Also overexpression of circRNA1615 could weaken the effect of miR-152-3p mimic, and the miR-152-3p mimic increased the hypoxia injury of LRP6 and Cx43, further LRP6 interference fragments could aggravate hypoxia injury of Cx43.(Fig.3 and Fig.4)

In previous reports, LRP6 focuses on lipid homeostasis and glucose metabolism associated with the rapamycin target protein (mTOR) pathway.[17] As we know, GNAS encodes the $G\alpha_s$ (stimulatory G-protein alpha subunit) protein, which mediates G protein–coupled receptor (GPCR) signaling. GNAS mutations cause developmental delay, short stature, and skeletal abnormalities in a syndrome called Albright's hereditary osteodystrophy. Because of imprinting, mutations on the maternal allele also cause obesity and hormone resistance (pseudohypoparathyroidism).[18,19] Importantly, ligand binding to certain heterotrimeric guanine nucleotide–binding protein (G protein)–coupled receptors (GPCRs) ligands induce the aggregation of LRP6 and cause the accumulation of $G\alpha_s\beta\gamma$ on the plasma member to set up a functional GPCR-$G\alpha_s$-AC complex for cyclic adenosine monophosphate (cAMP) generation and PKA activation. The activated PKA, on the one hand, phosphorylates LRP6 and accelerates the binding of G protein complexes to LRP6 to enable enhanced production of cAMP, on the other hand, it phosphorylates Cx43 and controls gap junction communication (Fig.7).[10, 20-22]

In the present study, LRP6 interference fragments could aggravate hypoxia injury of Cx43. The overexpression of LRP6 could significantly increase the protein level and phosphorylation level of Cx43, but the interference with LRP6 showed the opposite trend. Noticeably, the interference with $G\alpha_s$ weakened the protein and phosphorylation level of Cx43, however, interference with LRP6 and $G\alpha_s$ further inhibited the protein level and phosphorylation level of Cx43 (Fig.5). In addition, we also found that the transcriptions of circRNA1615 and LRP6 were inhibited in AMI, but the transcription of miR-152-3p was promoted, and the overexpression of circRNA1615 could weaken the damage effect and VT of AMI (Fig.6).

Limitations and Perspective: Noticeably, the dramatic decreases in gap junctional communication, and concomitant loss of phosphorylated Cx43 and accumulation of nonphosphorylated Cx43 have been reported in epithelial cells treated with 18b-glycyrrhetinic acid34 and glial cells exposed to oleamide.[23] The phosphorylation of serine residues in the carboxyl-terminal intracellular domain of Cx43 appears to be the major post-translation modification, and generalized loss of serine phosphorylation reflected by a shift to 41 kDa is associated with uncoupling,[23,24] however, the phosphorylation of tyrosine residues can occur in Cx43 and is also associated with uncoupling.[25,26] Currently, although we found that $G\alpha_s$ affected the dephosphorylation of Cx43 isoforms in VT induced by ischemia, future studies will be required to identify the precise pathophysiological relationship between the dephosphorylation at specific amino acid residues of Cx43 and uncoupling, and its potential effects on the development of VT in the peri-infarcted zone.

Conclusions LRP6 and its upstream genes circRNA1615 and miR-152-3p modulated the phosphorylation of Cx43 via Gαs in VT of MI.

Data Availability

The data used to support the findings of this study are available from the corresponding author upon request.

Ethical Approval

The study was approved by the ethics board of the Laboratory Animal Research Center, Tongji University (No. TJTJ00621401).

Disclosure

The funders did not play any roles in the design of the study, in the collection, analysis, and interpretation of data; and in writing the manuscript.

Conflicts of Interest

None of the authors have any potential conflict of interest to disclose.

Authors' Contributions

S.K. conceived and designed the study. X.M.Z, Y.L.L, and Y.H. participated in the experiment and in data collection. Y.C was responsible for quality control. S.K. analyzed data and drafted the manuscript. S.K., X.M.Z, and Y.L.L. participated in the fund support of the study. All of the authors have read and approved the manuscript.

Acknowledgments

This work was supported in part by projects of the National Natural Science Foundation of China (81870247 to S.K. and 81801936 to Y.L.L.), the General Program of Shanghai Municipal Science and

Technology Commission (20Y11910000, to X.M.Z), and the Top-Level Clinical Discipline Project of Shanghai Pudong District (Grant No. PWYgf 2021-01, to Y.H.C).

References

1. Hashimoto T, Ako J, Nakao K, et al. A lower eicosapentaenoic acid/arachidonic acid ratio is associated with in-hospital fatal arrhythmic events in patients with acute myocardial infarction: a J-MINUET substudy. Heart Vessels 2018;33(5):481-488.
2. Hasan W, Jama A, Donohue T, et al. Sympathetic hyperinnervation and inflammatory cell NGF synthesis following myocardial infarction in rats. Brain Res 2006;1124(1):142-154.
3. Aimond F, Alvarez JL, Rauzier JM, Lorente P, Vassort G. Ionic basis of ventricular arrhythmias in remodeled rat heart during long-term myocardial infarction. Cardiovasc Res 1999;42(2):402-415.
4. Disertori M, Masè M, Ravelli F. Myocardial fibrosis predicts ventricular tachyarrhythmias. Trends Cardiovasc Med 2017;27(5):363-372.
5. Scalise RFM, De Sarro R, Caracciolo A, et al. Fibrosis after Myocardial Infarction: An Overview on Cellular Processes, Molecular Pathways, Clinical Evaluation and Prognostic Value. Med Sci (Basel) 2021;9(1):16.
6. Roell W, Lewalter T, Sasse P, et al. Engraftment of connexin 43-expressing cells prevents post-infarct arrhythmia. Nature 2007;450(7171):819-824.
7. Mani A, Radhakrishnan J, Wang H, et al. LRP6 mutation in a family with early coronary disease and metabolic risk factors. Science 2007;315(5816):1278-1282.
8. Kang S. Low-density lipoprotein receptor-related protein 6-mediated signaling pathways and associated cardiovascular diseases: diagnostic and therapeutic opportunities. Hum Genet 2020;139(4):447-459.
9. Li J, Li C, Liang D, et al. LRP6 acts as a scaffold protein in cardiac gap junction assembly. Nat Commun 2016;7:11775.
10. Wan M, Li J, Herbst K, et al. LRP6 mediates cAMP generation by G protein-coupled receptors through regulating the membrane targeting of Gα(s). Sci Signal 2011;4(164):ra15.
11. Li RL, Fan CH, Gong SY, Kang S. Effect and Mechanism of LRP6 on Cardiac Myocyte Ferroptosis in Myocardial Infarction. Oxid Med Cell Longev 2021;2021:8963987.
12. Nagy JI, Li WE, Roy C, et al. Selective monoclonal antibody recognition and cellular localization

of an unphosphorylated form of connexin43. Exp Cell Res 1997;236(1):127-136.

13. Beardslee MA, Lerner DL, Tadros PN, et al. Dephosphorylation and intracellular redistribution of ventricular connexin43 during electrical uncoupling induced by ischemia. Circ Res 2000;87(8): 656-662.
14. de Diego C, Pai RK, Chen F, et al. Electrophysiological consequences of acute regional ischemia/reperfusion in neonatal rat ventricular myocyte monolayers. Circulation 2008;118(23): 2330-2337.
15. Schulz R, Görge PM, Görbe A, Ferdinandy P, Lampe PD, Leybaert L. Connexin 43 is an emerging therapeutic target in ischemia/reperfusion injury, cardioprotection and neuroprotection. Pharmacol Ther 2015;153:90-106.
16. Turner MS, Haywood GA, Andreka P, et al. Reversible connexin 43 dephosphorylation during hypoxia and reoxygenation is linked to cellular ATP levels. Circ Res 2004;95(7):726-733.
17. Labbé P, Thorin E. Therapeutic Targeting of LRP6 in Cardiovascular Diseases: Challenging But Not Wnt-Possible! Can J Cardiol 2019;35(11):1567-1575.
18. Mendes de Oliveira E, Keogh JM, Talbot F, et al. Obesity-Associated GNAS Mutations and the Melanocortin Pathway. N Engl J Med 2021;385(17):1581-1592.
19. Jüppner H. Obesity and Gαs Variants. N Engl J Med 2021;385(17):1619-1622.
20. Dukic AR, Gerbaud P, Guibourdenche J, Thiede B, Taskén K, Pidoux G. Ezrin-anchored PKA phosphorylates serine 369 and 373 on connexin 43 to enhance gap junction assembly, communication, and cell fusion. Biochem J 2018;475(2):455-476.
21. Dukic AR, Haugen LH, Pidoux G, Leithe E, Bakke O, Taskén K. A protein kinase A-ezrin complex regulates connexin 43 gap junction communication in liver epithelial cells. Cell Signal 2017;32: 1-11.
22. Ampey BC, Ampey AC, Lopez GE, Bird IM, Magness RR. Cyclic Nucleotides Differentially Regulate Cx43 Gap Junction Function in Uterine Artery Endothelial Cells From Pregnant Ewes. Hypertension 2017;70(2):401-411.
23. Guan X, Cravatt BF, Ehring GR, et al. The sleep-inducing lipid oleamide deconvolutes gap junction communication and calcium wave transmission in glial cells. J Cell Biol 1997;139(7): 1785-1792.
24. Guan X, Wilson S, Schlender KK, Ruch RJ. Gap-junction disassembly and connexin 43 dephosphorylation induced by 18 beta-glycyrrhetinic acid. Mol Carcinog 1996;16(3):157-164.

25. Li H, Spagnol G, Zheng L, Stauch KL, Sorgen PL. Regulation of Connexin43 Function and Expression by Tyrosine Kinase 2. J Biol Chem 2016;291(30):15867-15880.

26. Zheng L, Li H, Cannon A, et al. Phosphorylation of Cx43 residue Y313 by Src contributes to blocking the interaction with Drebrin and disassembling gap junctions. J Mol Cell Cardiol 2019;126:36-49.

Table 1. The sequences of siRNA used in the study

Name	Sense (5'-3')	Antisense (5'-3')
circRNA1615	AGUGACUUUAUUUUCCCAUTT	AUGGGAAAAUAAAGUCACUTT
LRP6	GCGGAUAUCAGACGCAUAUTT	AUAUGCGUCUGAUAUCCGCTT
GNAS	CAAUAAUAUGUCAGGACAATT	UUGUCCUGACAUAUUAUUGTT

Table 2. Primer sequences used in the study

Gene	Forward/Reverse	Sequence (5'-3')
miR-152-3p	Forward	CGCGTCAGTGCATGACAGA
	Reverse	AGTGCAGGGTCCGAGGTATT
U6	Forward	GCTTCGGCAGCAC
	Reverse	GGAACGCTTCACG
LRP6	Forward	TGCCCTGCCCACTACTCC
	Reverse	CAAGGTTCTGATTTGCGACTG
GNAS	Forward	CGAGAAGCAGCCGAGATGGAAG
	Reverse	GTGAGCATCGCGGAATCCGTAG
GAPDH	Forward	CTGCCCAGAACATCATCC
	Reverse	CTCAGATGCCTGCTTCAC

Figure legends

Figure1. Dephosphorylation of LRP6 and Cx43 were involved in ventricular tachycardia of AMI

(A) Micrographs of H&E-stained cardiomyocytes from the control and AMI mice. Scale bar: 100 μm. (B) LRP6 mRNA expressions assessed by real-time PCR assay in the control and AMI mice. (C) Phosphorylated LRP6 and CX43 expressions assessed by western blot assay in the control and AMI mice. (D) VT events were observed between AMI model and healthy control. Biological replication indicated three mice in each group.

Figure 2. The location and expression of circRNA1615 of LRP6 upstream gene in the control and AMI

(A) The location and expression of circRNA1615 in control and hypoxic cardiomyocytes assessed by FISH assay. Scale bar: 25 μm. (B) The location and expression of circRNA1615 in myocardial tissues from the control and AMI mice assessed by FISH assay. Scale bar: 50 μm. (C) circRNA1615mimic increased the expression of circRNA1615 in the cytoplasm assessed by FISH assay. Scale bar: 50 μm. Biological replication indicated three mice in each group

Figure 3. circRNA1615 regulates the effects of LRP6 and Cx43 via miR-152-3p in hypoxic cardiomyocytes.

(A, B) miR-152-3p levels in hypoxic cardiomyocytes treated with miR-152-3p inhibitor or mimic assessed by RT-qPCR. (C) Expression of Lrp6 in hypoxic cardiomyocytes treated with miR-152-3p inhibitor or mimic with or without circRNA1615 siRNA or pLVX-Puro-circRNA1615 assessed by RT-qPCR. (D) Expressions of LRP6 and CX43 in hypoxic cardiomyocytes treated with miR-152-3p inhibitor or mimic with or without circRNA1615 siRNA or pLVX-Puro-circRNA1615 assessed by Western blot. Pooled data: n= 3, n represents the number of experiments. ***$p<0.001$ vs. control; $^{\#\#}p<0.01$ vs. hypoxia; $^{\Delta\Delta}p<0.01$ vs. hypoxia+miR-152-3p inhibitor; $^{\Delta}p<0.05$ vs. hypoxia+miR-152-3p mimic.

Figure 4. circRNA1615 regulates the effects of LRP6 on the related protein expressions in hypoxic cardiomyocytes.

(A-D) LRP6 expression in hypoxic cardiomyocytes treated with Lrp6 siRNA (A, B) or pcDNA-Lrp6

(C, D) assessed by RT-qPCR. Right, typical blots; Left, pooled data. n= 3. n represents the number of experiments. Data are means±s.e.m. ***P<0.01 compared with control by two-tailed unpaired t-test. (E) Expression of LRP6, p-LRP6, Cx43 and p-Cx43 in hypoxic cardiomyocytes treated with Lrp6 siRNA or pcDNA-Lrp6 with or without pLVX-Puro-circRNA1615 or circRNA1615 siRNA assessed by Western blot. ***p<0.001 vs. control.

Figure 5. LRP6 and Gα_s regulate Cx43 and its phosphorylation levels.

(A) Expression of Cx43 and p-Cx43 in cardiomyocytes treated with Lrp6 siRNA or pcDNA-Lrp6 assessed by Western blot. (B) Expression of Gα_s in cardiomyocytes treated with Gnas siRNA assessed by RT-qPCR. (C) Expression of Gα_s, Cx43 and p-Cx43 in cardiomyocytes treated with Gnas siRNA with or without Lrp6 siRNA assessed by Western blot. Pooled data: n= 3, n represents the number of experiments.

Figure 6. circRNA1615 regulates miR-152-3p and related protein expressions in AMI mice.

(A) Micrographs of H&E-stained cardiomyocytes, the location and expression of circRNA1615 in myocardial tissues from the control, AMI, circRNA1615 and AMI plus circRNA1615 mice assessed by FISH assay. Scale bar: 100 μm. (B-D) VT events (B), miR-152-3p (C) and LRP6 (D) in myocardial tissues from the control, AMI, circRNA1615 and AMI plus circRNA1615 mice assessed by RT-qPCR. Pooled data: biological replication indicated three mice in each group. Expression of LRP6, p-LRP6, Cx43, and p-Cx43 in myocardial tissues from the control, AMI, circRNA1615 and AMI plus circRNA1615 mice assessed by Western blot. *p<0.05, **p<0.01, ***p<0.001 vs. control; $^{\#}$p<0.05, $^{\#\#}$p<0.01, $^{\#\#\#}$p<0.001 vs. AMI.

Figure 7. Mechanism schematic diagram.

circRNA1615 regulates the expression of LRP6 mRNA through sponge adsorption of miR-152-3p. GPCR ligands induce the aggregation of LRP6 and cause the accumulation of G$\alpha_s\beta\gamma$ on the plasma member to set up a functional GPCR-Gα_s-AC complex for cAMP generation and PKA activation. The activated PKA, on the one hand, phosphorylates LRP6 and accelerates the binding of G protein complexes to LRP6 to enable enhanced production of cAMP, on the other hand, it phosphorylates Cx43 and controls gap junction communication.

Note: AC, adenyl cyclase; ATP, adenosine triphosphate; CAMP, cyclic adenosine monophosphate; Cx43, connexin 43; Gαs, G-protein alpha subunit; G β s, G-protein Beta subunit; G γ s, G-protein gamma subunit; GPCR, G - protein - coupled receptor; LRP6, low density lipoprotein receptor related protein 6; PKA, protein kinase A.

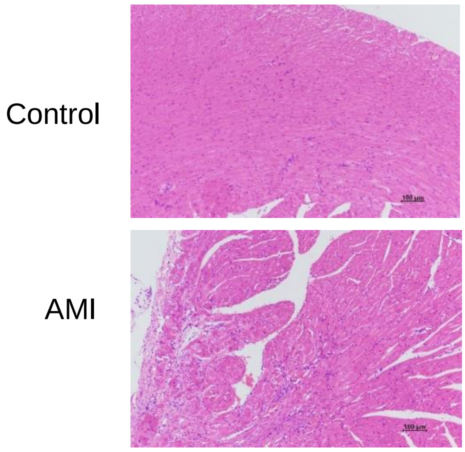

Figure 1(A).

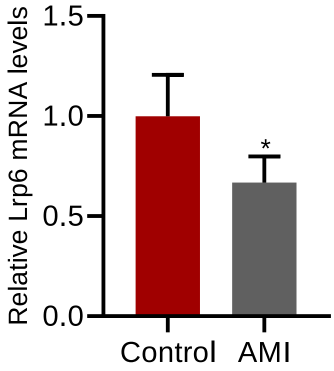

Figure 1(B).

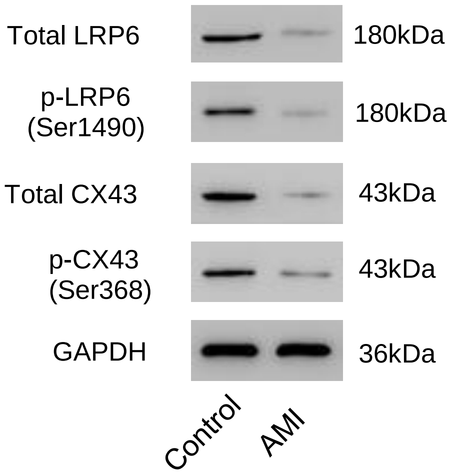

Figure 1(C).

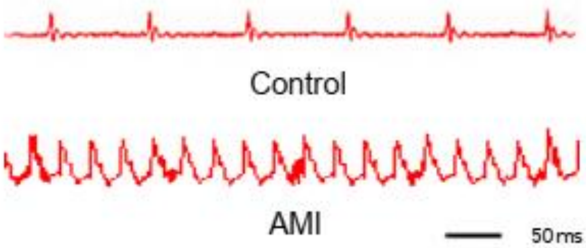

Figure 1(D)

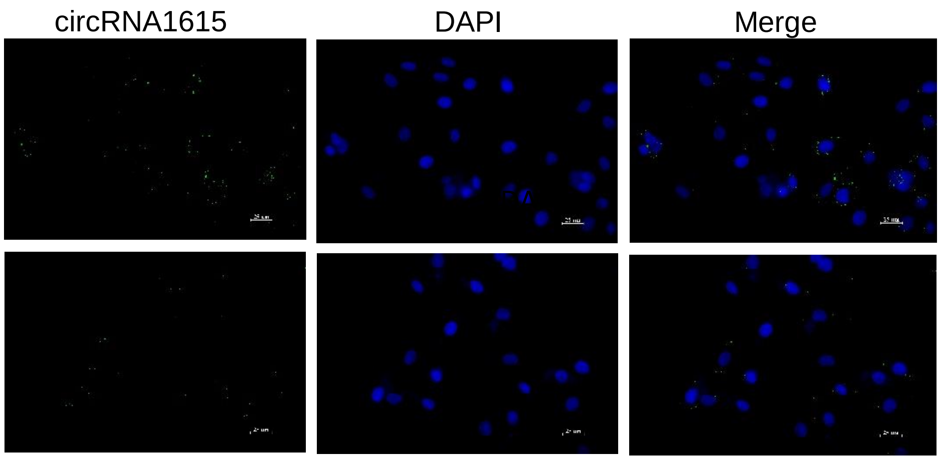

Figure 2 (A).

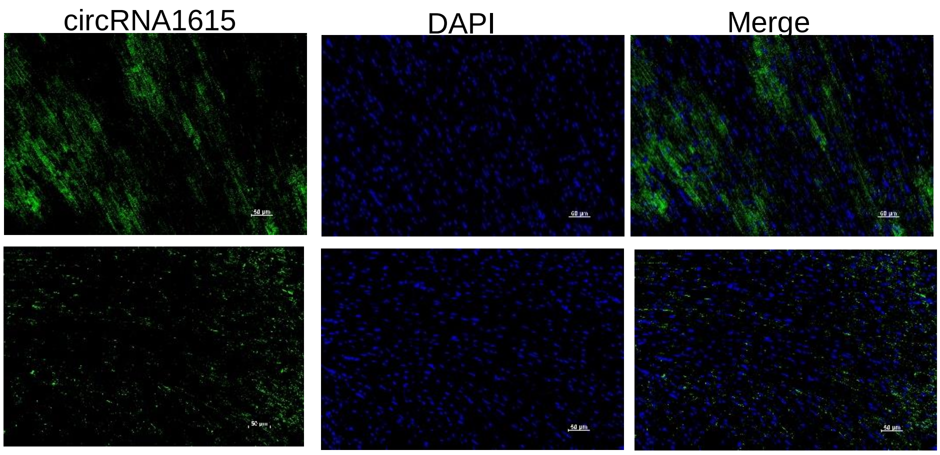

Figure 2 (B).

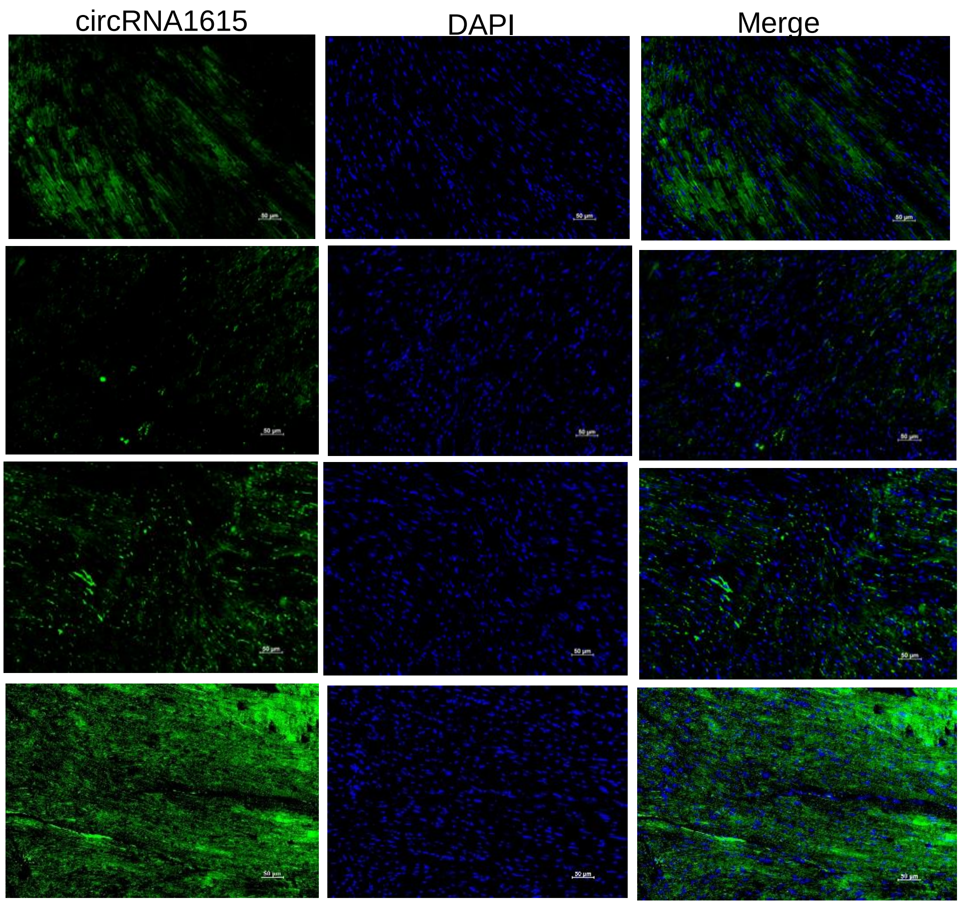

Figure 2 (C).

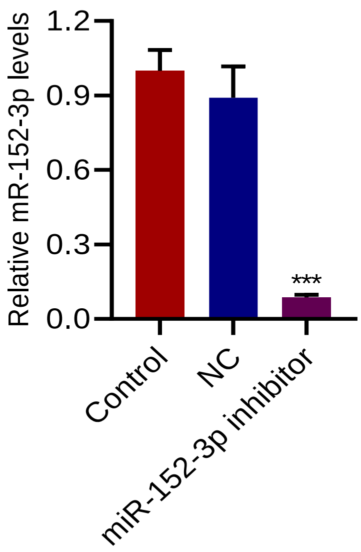

Figure 3(A).

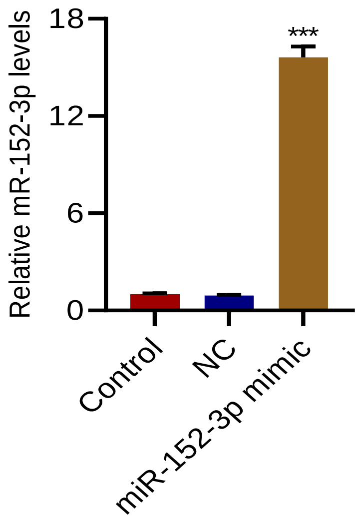

Figure 3(B).

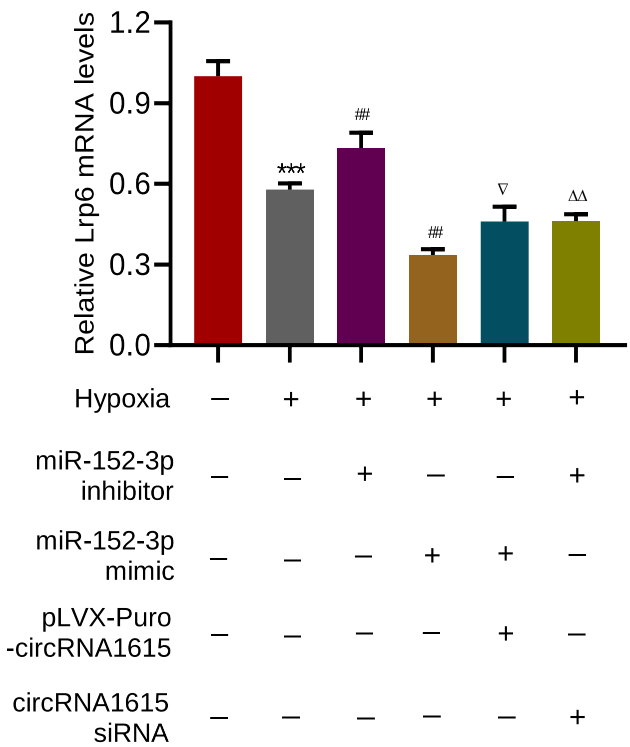

Figure 3(C).

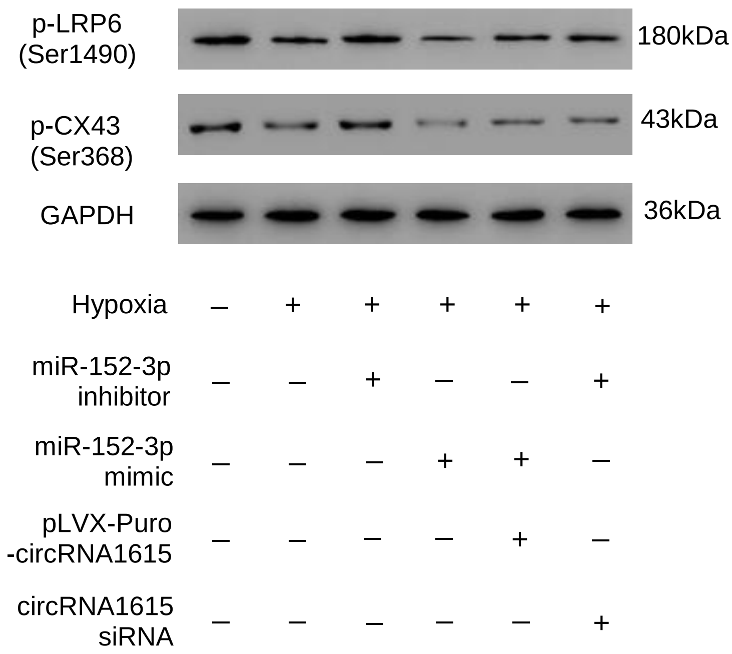

Figure 3(D).

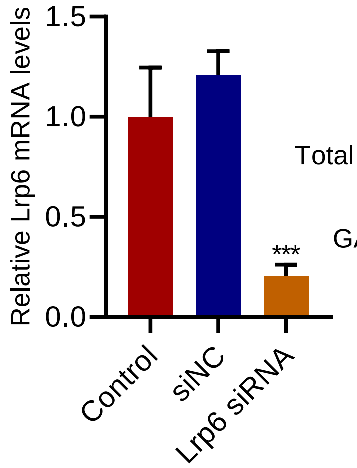

Figure 4(A).

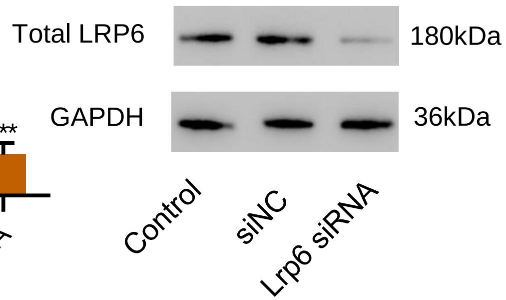

Figure 4(B).

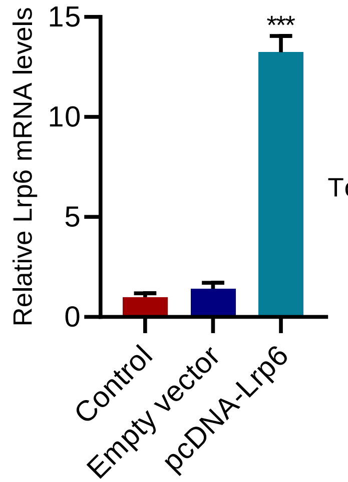

Figure 4(C).

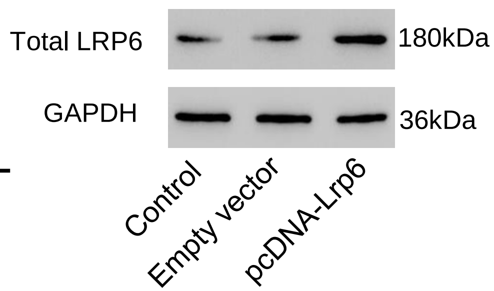

Figure 4(D).

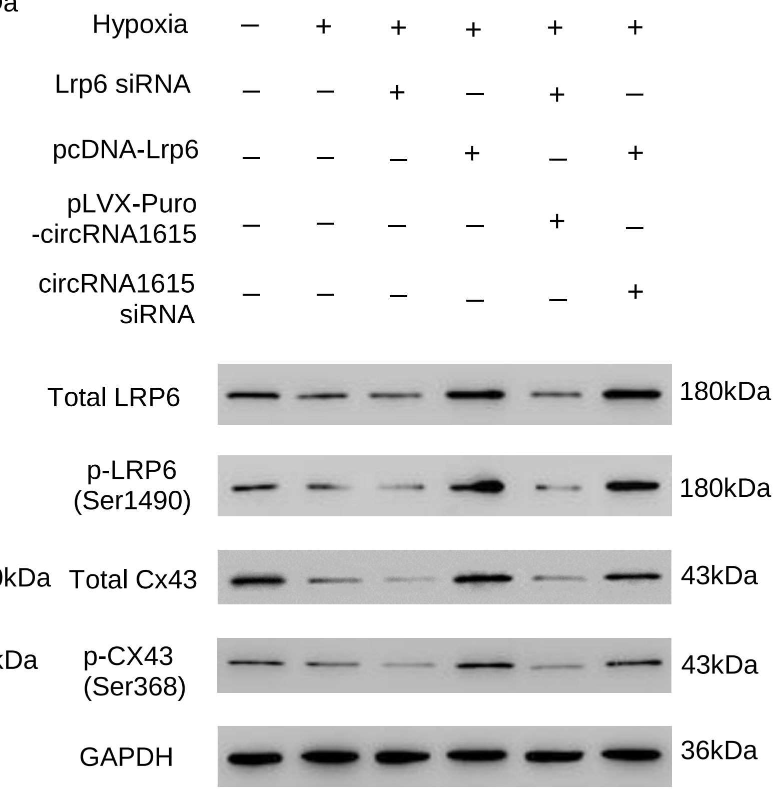

Figure 4(E).

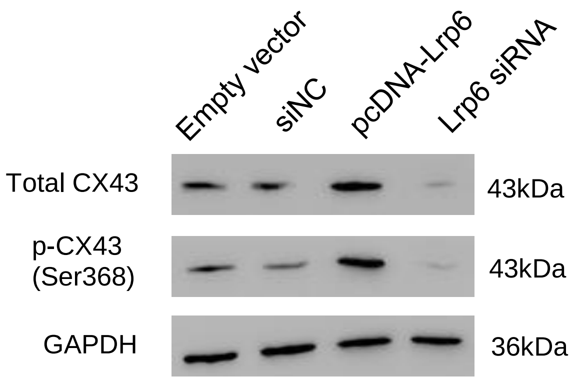

Figure 5(A).

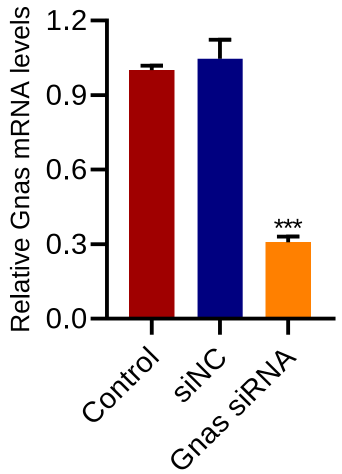

Figure 5(B).

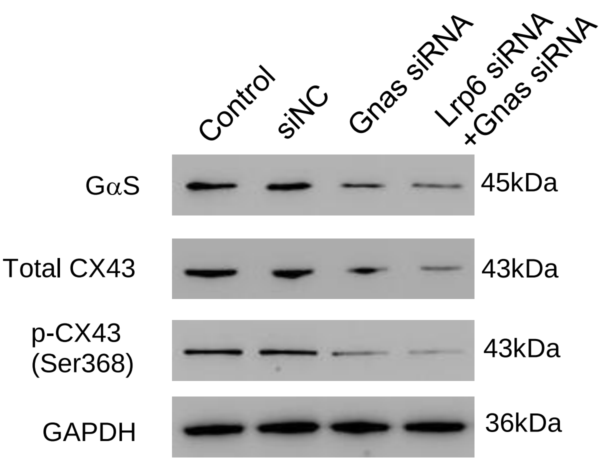

Figure 5(C).

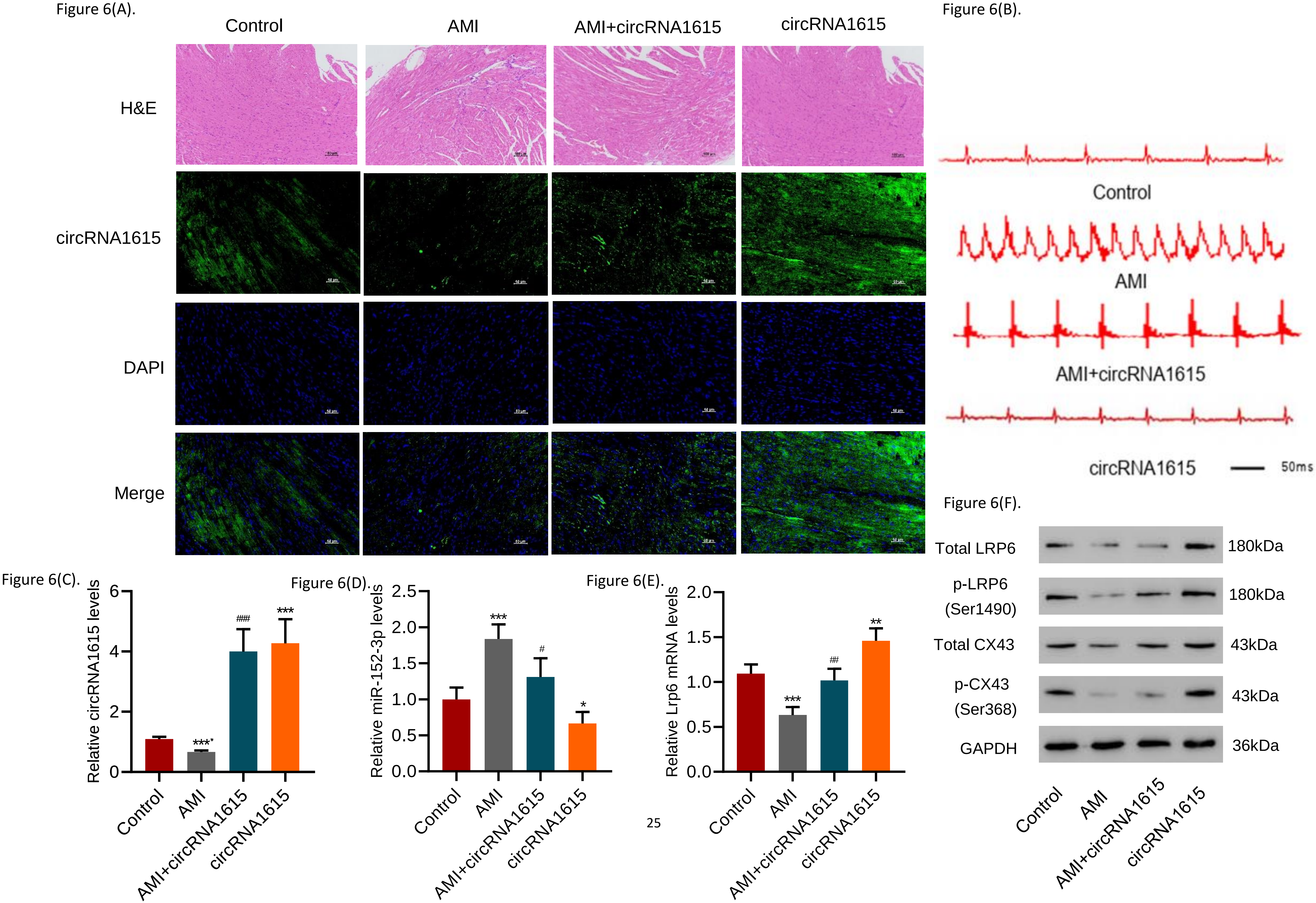

Figure 6(A).
Control
AMI
AMI+circRNA1615
circRNA1615
H&E
circRNA1615
DAPI
Merge
Figure 6(B).
Control
AMI
AMI+circRNA1615
circRNA1615
50ms
Figure 6(C).
Relative circRNA1615 levels
***
###
***
Control
AMI
AMI+circRNA1615
circRNA1615
Figure 6(D).
Relative miR-152-3p levels
***
#
*
Control
AMI
AMI+circRNA1615
circRNA1615
Figure 6(E).
Relative Lrp6 mRNA levels
***
##
**
Control
AMI
AMI+circRNA1615
circRNA1615
Figure 6(F).
Total LRP6
180kDa
p-LRP6 (Ser1490)
180kDa
Total CX43
43kDa
p-CX43 (Ser368)
43kDa
GAPDH
36kDa
Control
AMI
AMI+circRNA1615
circRNA1615

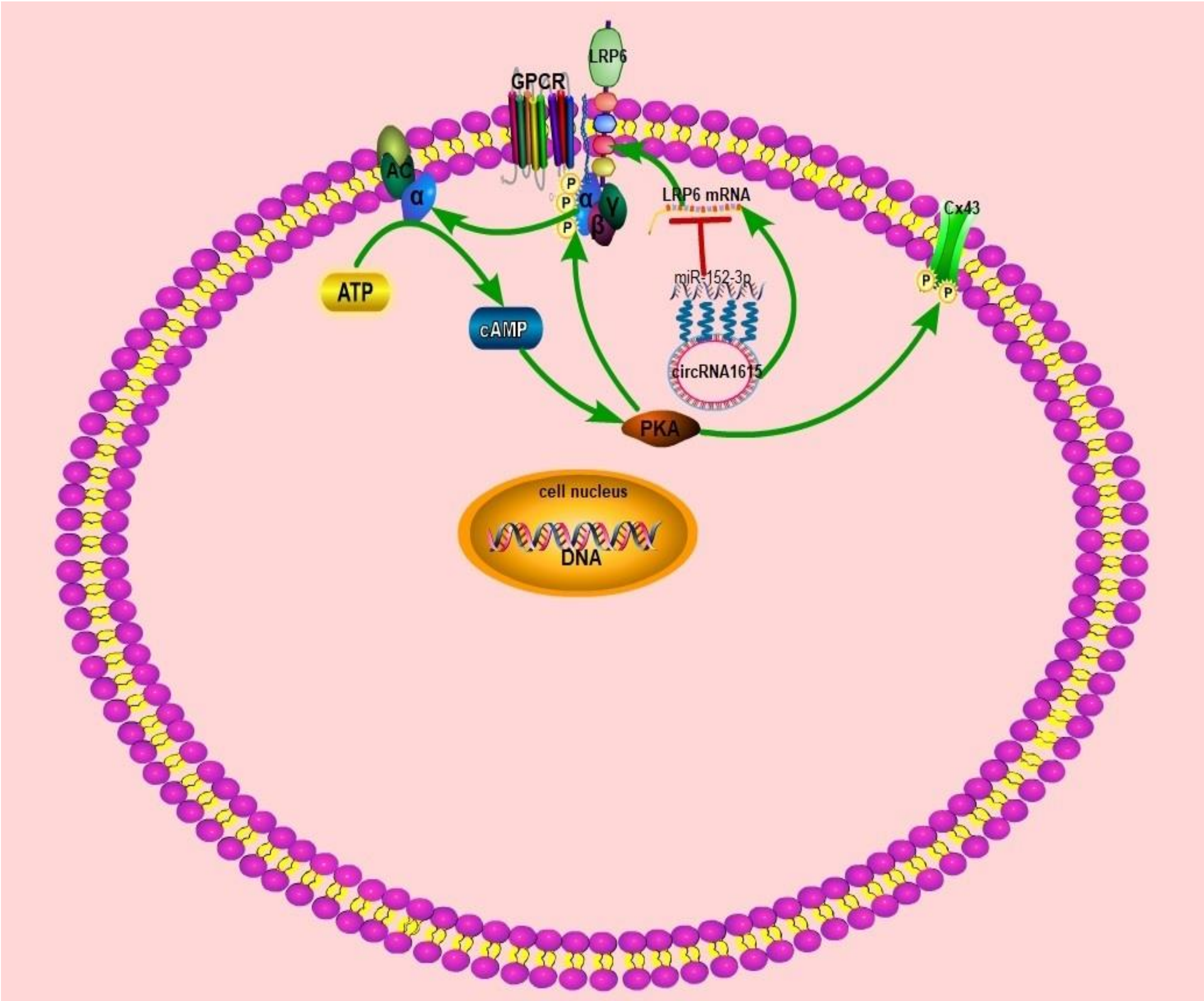

LRP6
GPCR
AC
α
P
P
P
P
α
γ
β
LRP6 mRNA
miR-152-3p
Cx43
P
P
ATP
cAMP
circRNA1615
PKA
cell nucleus
DNA

Figure 7.